Relations between electrical resistivity, carbon dioxide flux, and self-potential in the shallow hydrothermal system of Solfatara (Phlegrean Fields, Italy)

S. Byrdina [a,*], J. Vandemeulebrouck [a], C. Cardellini [b], A. Legaz [a], C. Camerlynck [c], G. Chiodini [d], T. Lebourg [e], M. Gresse [a], P. Bascou [a], G. Motos [a], A. Carrier [a], S. Caliro [d]

[a] ISTerre, Université de Savoie, Equipe Géophysique des Volcans, IRD R219, CNRS, UMR 5275, F-73376 Bourget du Lac, France
[b] University of Perugia, Italy
[c] Sorbonne Université, UPMC - Université Paris 6, UMR 7619 Metis, 75005 Paris, France
[d] Istituto Nazionale di Geofisica e Vulcanologia, Sezione di Napoli, Osservatorio Vesuviano, Via Diocleziano 328, 80124 Napoli, Italy
[e] Géoazur, UMR7329, France

ARTICLE INFO

ABSTRACT

We present the results of an electric resistivity tomography (ERT) survey, combined with mappings of diffuse carbon dioxide flux, ground temperature and self-potential (SP) at Solfatara, the most active crater of Phlegrean Fields. Solfatara is characterized by an intense carbon dioxide degassing, fumarole activity, and ground deformation. This ensemble of methods is applied to image the hydrothermal system of Solfatara, to understand the geometry of the fluid circulation, and to define the extension of the hydrothermal plume at a high enough resolution for a quantitative modeling. ERT inversion results show Solfatara as a globally conductive structure, with resistivity in the range 1–200 Ω m. Broad negative anomaly of self-potential in the inner part of Solfatara with a minimum in the area of Bocca Grande suggests a significant downward flow of condensing liquid water. Comparison between spatial variations of resistivity and gas flux indicates that resistivity changes at depth are related to gas saturation and fluid temperature. These variations delineate two plume structures: a liquid-dominated conductive plume below Fangaia mud-pool and a gas-dominated plume below Bocca Grande fumarole. The geometry of the Fangaia liquid-saturated plume is also imaged by a high resolution 3-D resistivity model. In order to estimate the permeability, we propose a 2-D axis-symmetric numerical model coupling Richards equation for fluid flow in conditions of partial saturation with the resistivity calculation as function of saturation only. Alternatively, we apply the Dupuit equation to estimate the permeability of the shallow layer. Using these two approaches we obtain the permeability of the shallow layer below Fangaia which ranges between $(2–4) \times 10^{-14}$ m^2.

1. Introduction

The Phlegrean Fields (Campi Flegrei) is a volcanic complex located in a densely populated area to the West of Naples in Italy (Fig. 1a). The recent activity of this resurgent caldera is characterized by repeated episodes of large ground deformation, seismicity associated to uplift episodes, intense diffuse degassing, and fumarolic emissions (e.g. Chiodini et al., 2005; Chiodini et al., 2009; Todesco et al., 2010). According to Chiodini et al. (2001), about 1500 tons of CO_2 and >3000 tons of a water vapor are released per day at Solfatara, presently the most active crater of Phlegrean Fields. A major part of the emitted water vapor is condensed at the near surface producing a thermal power flux around 100 MW, and contributing substantially to the total water input into the hydrothermal system (Chiodini et al., 2005). The geochemical analysis of Solfatara fumarolic gases performed by Caliro et al. (2007) indicates that deep magmatic CO_2-rich fluids mix with hydrothermal liquids of meteoric origin and form a hydrothermal plume that feeds the fumaroles of Solfatara. The geometry of this hydrothermal plume between 0 and 2500 m deep was delineated by de Siena et al. (2010) as corresponding to an area of high seismic attenuation. The magmatic body supplying heat to this hydrothermal plume was identified by seismic reflection studies at 7.5 km below the surface (Zollo et al., 2008). The influence of the hot H_2O–CO_2 gas source underneath Solfatara on the deep hydrothermal fluid circulation was modeled by Petrillo et al. (2013) using the TOUGH2 multi-component transport code simulator. This 3-D model accounts for water table topography and bathymetry over the area. The permeability structure, with values ranging from 5×10^{-17} to 7×10^{-14} m^2, with the highest values at shallowest depths, was obtained using empirical relations between density and porosity and between porosity and permeability.

* Corresponding author.
  E-mail addresses: svetlana.byrdina@univ-savoie.fr (S. Byrdina),
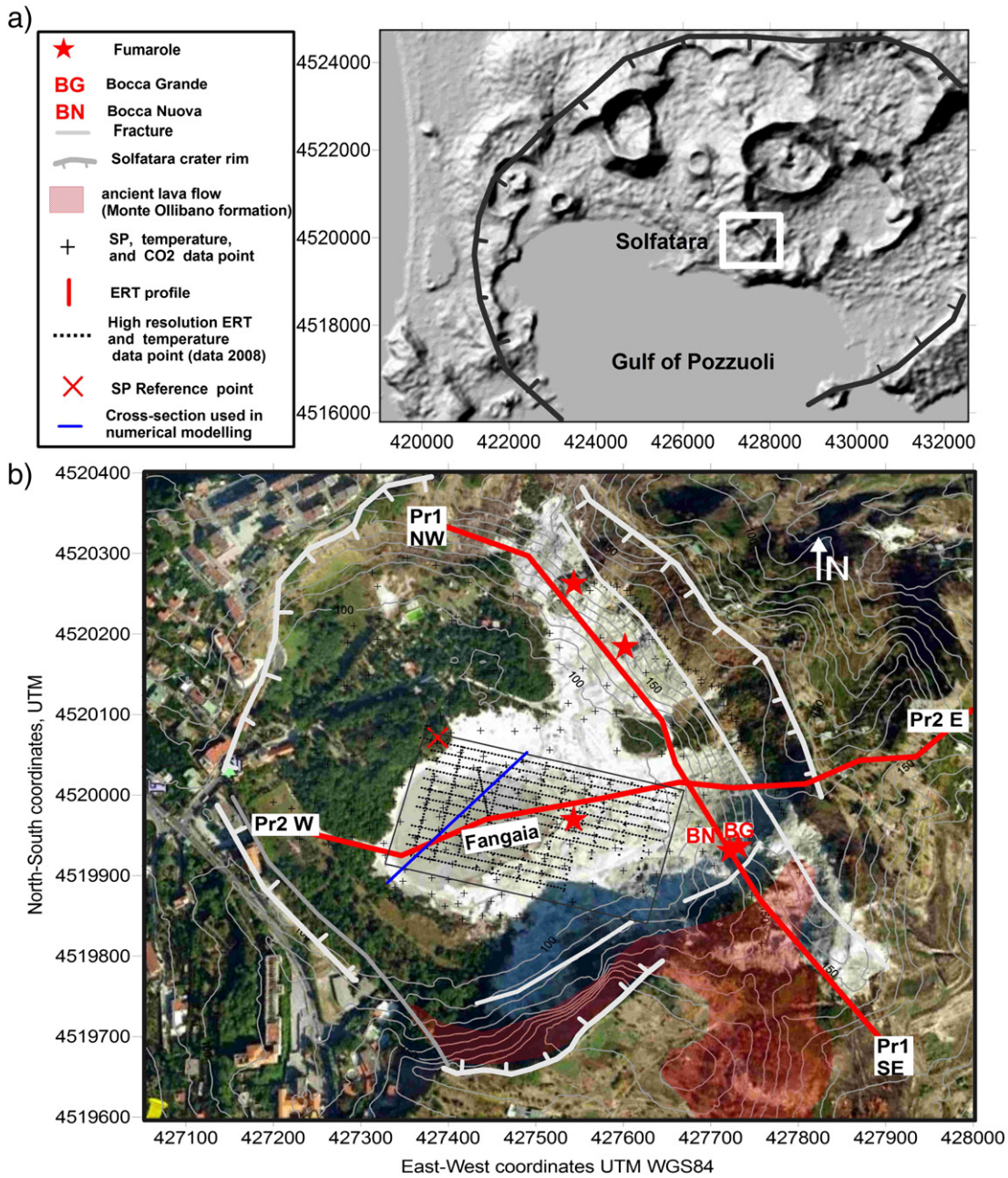Jean.Vandemeulebrouck@univ-savoie.fr (J. Vandemeulebrouck).

Fig. 1. Location of Solfatara at Phlegrean Fields, with main geological structures (after Lirer et al., 2011), and localization of the study area. The two 1 km-long ERT profiles are indicated by red solid lines, and blue solid line shows the orientation of the cross-section of 3-D resistivity model used for permeability estimations (Fig. 11). Dotted lines indicate the 23 short-length ERT profiles used to perform the 3-D model. The SP reference point is indicated by the large red cross.

Bruno et al. (2007) performed geophysical surveys inside Solfatara and hydrogeological measurements in 30 boreholes in the surroundings, in order to recognize the upper structure of the hydrothermal plume. The water table positions clearly identify the upwelling of the piezometric surface, with the maximum below Solfatara crater, produced by the plume. Their geophysical surveys in Solfatara crater, including a CSAMT (controlled source audio magneto-tellurics) and several ERT profiles, showed the presence of a conductive layer overlain by a shallow resistive vadose layer in the center of Solfatara. Using a numerical thermodynamic model, Rinaldi et al. (2011) reproduced the main electrical resistivity features observed at Solfatara, and demonstrated that the range of resistivity observed by Bruno et al. (2007) at shallow

depths can be explained in terms of gas ratio and temperature variations in the porous geological structure.

The present study aims to complete the previous geophysical campaigns at Solfatara in order to obtain a high-resolution image of the shallow hydrothermal structures. We performed two kilometer-long ERT profiles coupled to self-potential, soil temperature and CO_2 flux measurements. This multi-method approach possesses a significant potential for recognizing the structure of hydrothermal systems (e.g. Revil et al., 2004; Revil et al., 2008; Finizola et al., 2010). Our investigation covers the Solfatara crater and includes the area of intensive degassing on the crater rims and the Bocca Grande fumarole. From our results, we propose a conceptual model of the shallow

hydrothermal circulation. A detailed geophysical survey using 24 ERT profiles was also performed on the central mud pool Fangaia area, where CO_2-rich liquid water reaches the surface. The sub-surface structure of this high-conductivity liquid plume allowed us to estimate the permeability of the first 15 m depth of soil.

2. Data basis and observations

Self-potential (SP) measurements were performed in May 2011 using non-polarizable Pb/PbCl$_2$–NaCl electrodes (Petiau, 2000) and a high impedance Fluke 27 II voltmeter. The weather was sunny without any rainfall, the soil was nevertheless wet enough to ensure a good electrical contact due to condensation of degassed vapor. The reference electrode was placed in a location without any hydrothermal manifestations at the surface where the carbon dioxide flux was close to the background value (Fig. 1b). SP mapping was carried out in an area of approximately 500 m × 500 m and included over 400 data points (Fig. 1).

A high resolution mapping of the ground temperature at 15 cm depth was performed in May 2011 in the whole area of Solfatara, and in May 2009 in the area around the Fangaia mud pool. In total, almost 1000 measurements of the ground temperature where used to produce our map. Although the recent monitoring studies (e.g., Chiodini et al., 2009) show an increase of hydrothermal activity at Solfatara, the
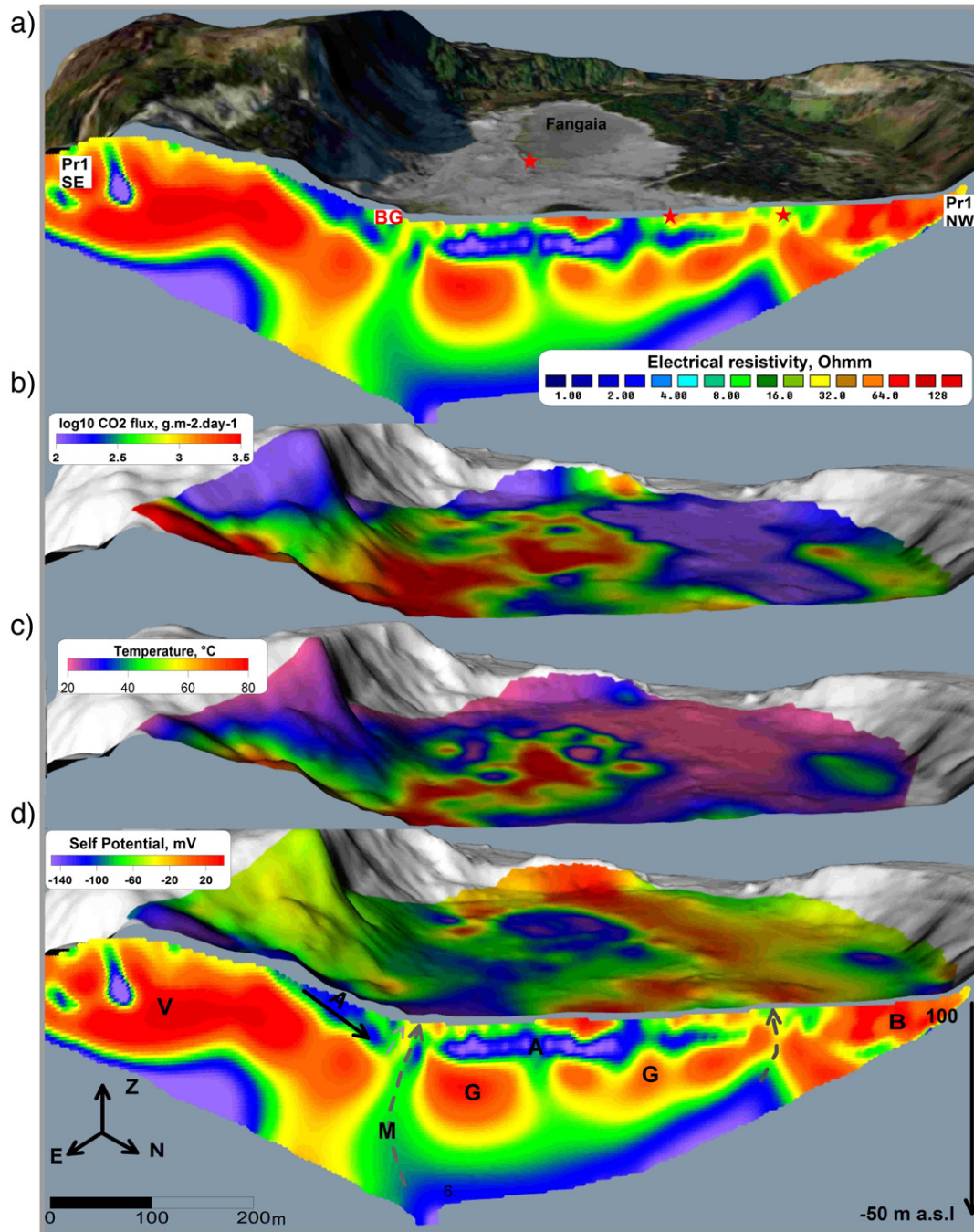

Fig. 2. 2-D resistivity vertical cross-section along profile 1 compared to a) Google Image draped over a DEM of the area, b) logarithm of the carbon dioxide distribution (in g m^{-2} day^{-1}), c) ground temperature at 15 cm depth in °C, and d) self-potential in mV. Conceptual model with liquid water flow indicated by solid lines, gas flow indicated by dashed lines. The principal units are 'V' — vadose zone below the crater rim, 'A' — aquifer, 'G' — gas dominated reservoir, 'M' — the mixture of CO_2 and/gaseous/liquid water, 'B' — undisturbed area.
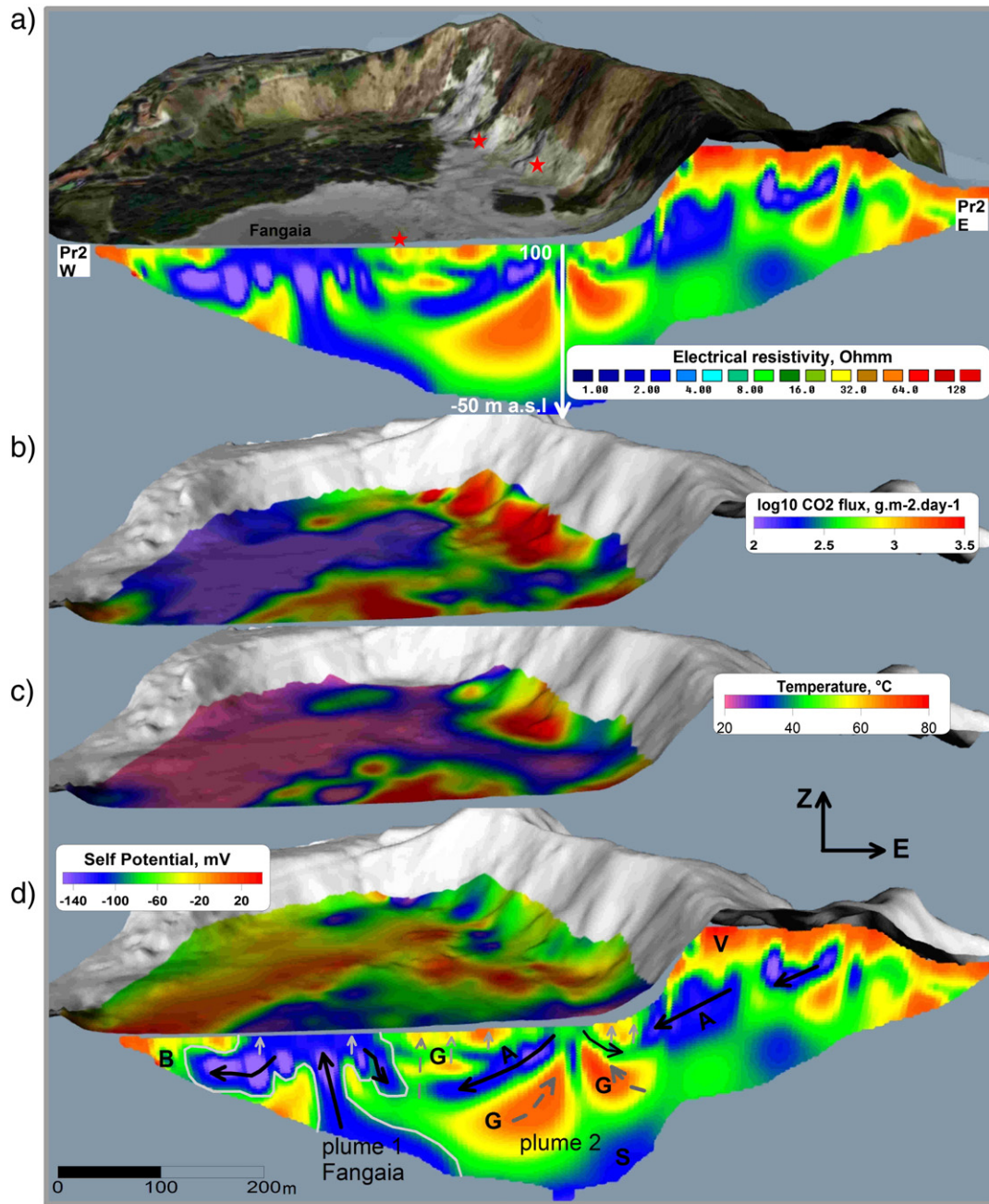
Fig. 3. Model and data representation as in Fig. 2 along profile 2. Subfigures a, b, c, and d have the same signification as in Fig. 2. Parameter H_0 of Dupuit equation in Eq. (1) in the case of unconfined flow is shown with white color. The resistivity variation delineates two plume structures: a liquid-dominated conductive plume below Fangaia (Plume 1) and a gas-dominated plume below Bocca Grande fumarole (Plume 2).

temperature measurements in Fangaia area in 2011 and 2009 are quite consistent and show the same average value. Therefore we decided to merge the data in a single map. Carbon dioxide fluxes were measured in May 2011 using accumulation chamber method detailed by Chiodini et al. (1996) and Chiodini et al. (1998). Data interpolation of SP, temperature, and CO_2 flux data, shown in Figs. 2–4, was performed using kriging interpolation technique.

In March 2008, 24 ERT profiles with length varying between 190 and 380 m were carried out in Fangaia area in two orthogonal directions in order to create a 3-D resistivity image. In May 2012, two 1-km-long profiles 1 and 2, a NW–SE and an E–W, were carried out across the caldera. Electrical resistivity tomography (ERT) was performed with an IRIS Syscal Pro Switch instrument; we used Wenner–Schlumberger

configuration for all profiles. Profiles 1 and 2 shown in Fig. 1 have a total length of 960 m each and a 10 m electrode spacing. Profile 1 has NW–SE orientation crossing the Southern rim of Solfatara and Bocca Grande fumarolic area. Profile 2 is West–East oriented and it crosses the Fangaia mud pool following the direction to the Pisciarelli fumarole (outside Fig. 1) and is roughly perpendicular to the NW–SE oriented fault on the eastern flank.

We performed a 2-D inversion of profiles 1 and 2. A 2-D approximation of Solfatara structure is easily acceptable for profile 2 which passes perpendicular to the main NW–SE fracture and associated fumarolic area. A 2-D approximation for profile 1 is less obvious, but as we show below in Section 4, the results of 2-D inversion for both profiles are remarkably consistent and give coherent information about common
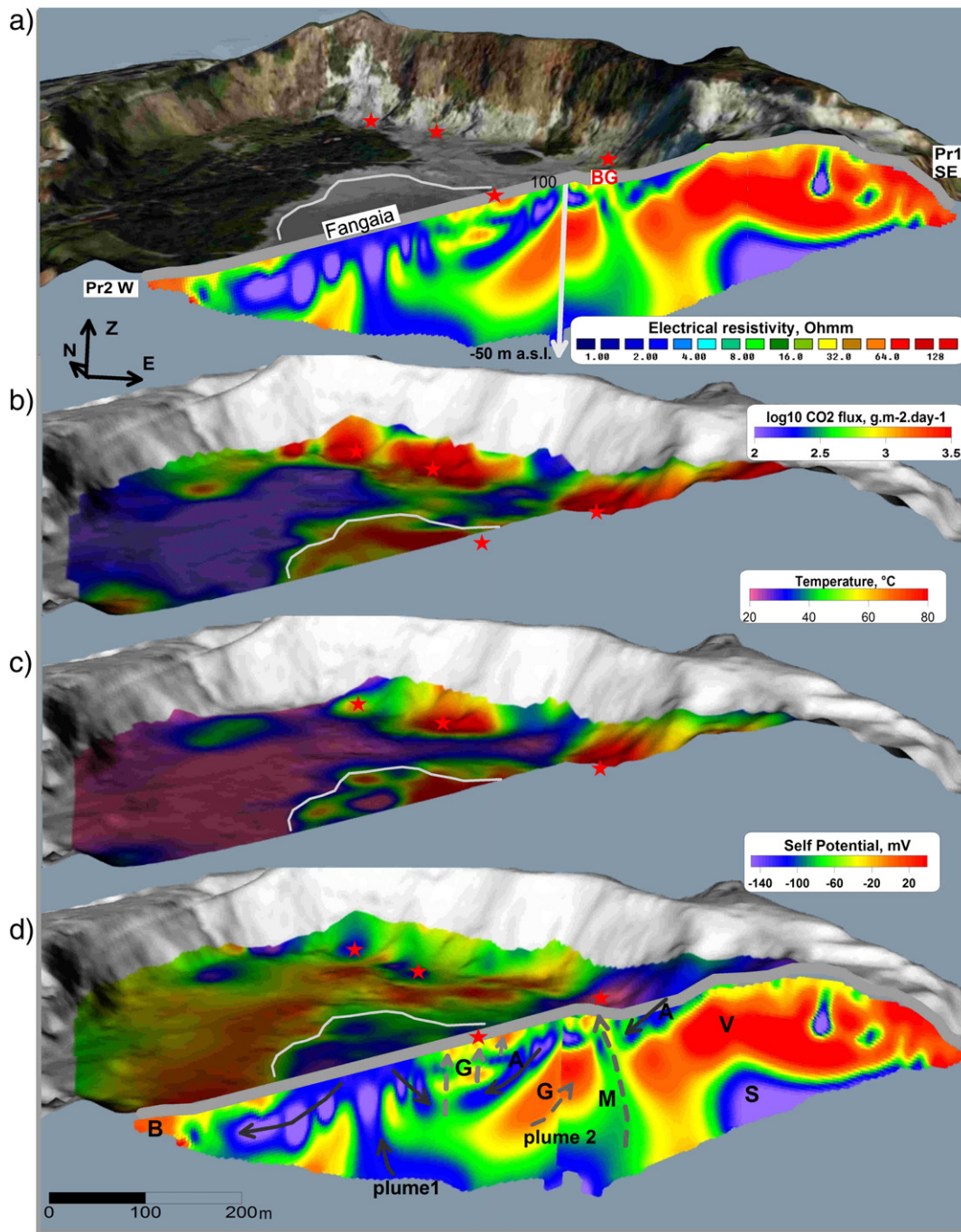
Fig. 4. View from the South at electric resistivity tomography models along profiles 1 and 2 assembled together with complementary data as in Figs. 2 and 3. Subfigures a, b, c, and d have the same signification as in Fig. 2. The principal units are 'V' — vadose zone below the crater rim, 'A' — aquifer, 'G' — gas dominated reservoir, 'M' — the mixture of CO_2 and/gaseous/liquid water, 'B' — undisturbed area.

gas-rich structures below Bocca–Grande fumarole imaged by both profiles. The 2-D data inversion was performed using RES2DINV (Loke and Barker, 1996), taking into account the topography in the inversion of the apparent resistivity data. The normalized RMS errors were close to 5% at the fifth iteration for the two profiles: 5.2% for profile 1 and 4.6% for profile 2. Pseudosections and model results for both profiles are shown in the Supplementary material, in Figs. S1 and S2. The maximal depth of penetration on the ERT profiles is about 150 m below the surface due to the low-resistivity of the medium.

A high resolution 3-D resistivity survey was performed in addition to these long 2-D profiles, in a zone of pronounced variations of piezometric surface around Fangaia. The area covered by 3-D ERT survey is

marked by a black thin rectangle in Fig. 1. ERT measurements were performed along 12 profiles with ESE–WNW orientation and 380 m length, and along 12 orthogonal profiles with NNE–SSW orientation and 180 m length. We used Wenner–Schlumberger (WS) and Dipole–Dipole (DD) configurations which gave similar results (Figs. S3–S4). The normalized RMS error of the 2D ERT inversion for most profiles varied between 1 and 5% (Figs. S5–S6 show two examples of ERT data and model sections for two orthogonal directions, WS configuration). 3-D inversion of the profiles was obtained using an algorithm detailed by Loke and Barker (1996) and implemented in RES3DINV software. The normalized RMS error of resulting 3-D model was better for WS than for DD configuration (6.8% and 10% respectively) as shown in Figs. S3–S4, therefore we

used the WS model in further analysis. The data quality allowed a high resolution modeling up to 15 m depth.

3. Results

3.1. Geophysical mapping

Results of the geophysical mapping and of the 2-D inversions of the ERT data are shown in Figs. 2–4. Generally, in the non-vegetated areas, CO_2 fluxes are high (>1000 g m^{-2} day^{-1}) and correlated with ground temperatures >40 °C (Figs. 2–4a, b, c). Extremely high CO_2 fluxes (>500 g m^{-2} day^{-1}) were measured close to the NW–SE fracture and between Fangaia and Bocca Grande, in agreement with previous studies in this area (e.g. Granieri et al., 2010). Remarkably, the self-potential anti-correlates with the gas flux and temperature data, with values < − 100 mV around each fumarole as well as around the Fangaia mud pool (Figs. 2–4d, 5). The lowest self-potential value (−160 mV) is found close to Bocca Grande fumarole.

Background values of the CO_2 fluxes (<500 g m^{-2} day^{-1}) and ground temperature (<30 °C) are observed exclusively in the vegetated areas. The self-potential takes there values from zero to few tens of mV with little variation.

An overall relationship between the CO_2 flux, ground temperature and self-potential is displayed in Fig. 5. The positive correlation between the ground temperature and the carbon dioxide flux can be described in the first approximation by a power law, whereas self-potential clearly anti-correlates with temperature and CO_2 flux.

3.2. ERT profiles

The inverted resistivities vary between 1 and 500 Ω m along profile 1 (Fig. 2) and between 1 and 200 Ω m along profile 2 (Fig. 3) indicating a near surface of Solfatara as a globally conductive structure. The highest resistivities we observed at Solfatara are one order of magnitude lower than the highest values obtained on Vulcano (Revil et al., 2008; Revil and Florsch, 2010) or Stromboli (Revil et al., 2011) where resistivity of massive lava units can reach 5000 Ω m. It is worth noting that the whole studied area is covered by tuff deposits and conglomerates that constitute a rock matrix of several tens of meter thick. Apart from a lava dome area of small extension that is lateral to our profile 1 (Fig. 1b), the geological units at shallow depth consist of the same tuff deposits, but characterized by different fluid composition and temperature. Therefore, we suggest that the resistivity variations at shallow depth also originate from the fluid composition, gas ratio and temperature, and rock alteration. The interpretation of the different

units that we propose below lies on the analysis of all the observed parameters (resistivity, self-potential, temperature and CO_2 flux).

To simplify the comparison between the different kinds of data displayed in Figs. 2–4, we show twice each ERT profile — together with: a) a Google Earth image, and d) together with the self-potential distribution. A conceptual model of the fluid flow presented by arrows in Figs. 2–4d is discussed below in Section 4.

The main structures of profile 1 are:

(1) Unit V (Vadose zone on the crater rims): a resistive body (200–500 Ω m) on the crater rim (SE part of profile). High gas fluxes and temperatures in this area suggest a low degree of water saturation and the presence of unconsolidated fractured rock or permeable deposits. This zone displays the highest resistivity values of the whole studied area and might correspond to an ancient lava flow (Monte Olibano formation in Fig. 1, Lirer et al., 2011).
(2) Unit A (Aquifer): a conductive layer (0.5–5 Ω m) in a depth of 20–50 m, interpreted as aquifer in Fig. 2d.
(3) Unit G (Gas): several bodies characterized by resistivity 50–100 Ω m below Bocca Grande and the NW–SE fracture attributed to high CO_2 saturation because of its vicinity to the fumaroles. Interestingly, these bodies are generally overlain by the conductive aquifer.
(4) Unit M (Mixture of water and gas): a vertical channel exactly below Bocca Grande fumarole (≈20 Ω m) associated with high ground temperatures and the absolute minimum of self-potential. This channel likely represents a pathway for the mixture of hot CO_2, vapor and condensing water.
(5) Unit B (Background): a high resistivity layer (up to 200 Ω m) at the NW extremity of the profile, below the vegetation cover and associated with background values of ground temperature and gas flux. This layer might correspond to non-saturated sands and tuffs relatively undisturbed by the hydrothermal activity.
(6) Unit S (Saline water conductor): a conductive layer (<3 Ω m) at the bottom of both profiles which can correspond to the water-saturated sediments (tuff) with possible mixing of sea water (Valentino et al., 1999).

Units V, A, G and S are imaged by profile 2 as well: V is a shallow resistive structure (200 Ω m) on the crater rim on the E-side of the profile; the lower resistivity in comparison to profile 1 suggests a higher degree of alteration; A is an ensemble of aquifers on the E-slope in the depth of 20–50 m; G is a gas-rich structure at a depth of 30–100 m below Bocca Grande. Despite the strong assumptions of a 2-D geometry of Solfatara area, inversions of both profiles image this gas-saturated structure with a remarkable agreement on its location and the value of resistivity. Profile 2 shows on its W-side what we consider as a spectacular image of a conductive hydrothermal plume in clay-rich environment (<5 Ω m) below the Fangaia mud pool. The location of the aquifers clearly follows the slope towards West, and the shape of the hydrothermal plume suggests a pronounced influence of local topography. Significant deviations of the hydrothermal circulation caused by a gradient of topography have been observed at different scales (Byrdina et al., 2013; Petrillo et al., 2013).

4. Discussion

4.1. Relation between electric resistivity, ground temperature, CO_2 flux and self-potential

The relationships between the resistivity structure and ground temperature, gas flux and self-potential are complex but some principal features can be recognized, especially on profile 2 which crosses the main hydrothermal structures of the area: Fangaia, Bocca Grande fumarole, the NW–SE fault, and the crater rim. While the slopes of the crater rim are characterized by a high resistivity typical of a vadose zone, a shallow conductor (<5 Ω m) is found in the inner part of Solfatara, below the area characterized by high temperatures and gas fluxes as well as
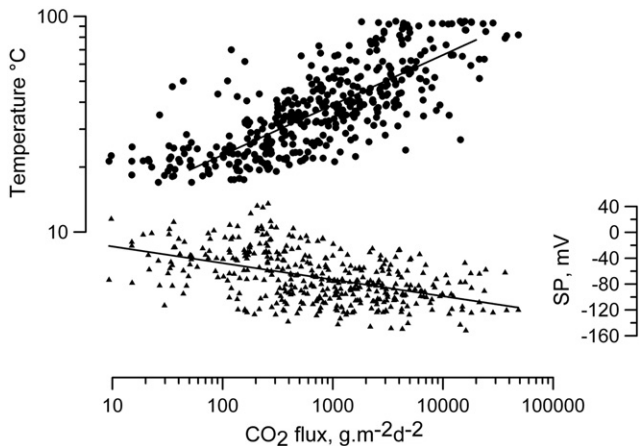

Fig. 5. Relationship between the ground temperature at a depth of 15 cm (in °C, top, dots), self-potential (in mV, bottom, triangles) and carbon dioxide flux (in g m^{-2} day^{-1}) for the whole studied area.

negative anomalies of self-potential (Figs. 2–4). This conductor lies on the top of a more resistive body (20–100 Ω m). Similar observations of a conductor systematically overlaying a more resistive body were reported in a vapor-saturated hydrothermal system in Yellowstone (Zohdy et al., 1973) or in Waimangu, New Zealand (Legaz et al., 2009). As in Zohdy et al. (1973), we suggest the conductor to represent an aquifer saturated with hot water condensing from a gas reservoir below (Petrillo et al., 2013). The interface between the resistivities typical for liquid water (0.5–5 Ω m) and gas (>20 Ω m) is about 30 m in the flat part of Solfatara which lies at a depth of ~30 m (Fig. 2). The average value of conductivity down to this depth is positively correlated with the gas flux/ground temperature as shown in Figs. 7 and 8. This positive correlation between conductance and degassing illustrates a close relationship between the presence of condensate rich aquifers and deeper fumarole-feeding gas dominated structures (the higher electrical resistivity of which does not influence the conductance of the shallow layer). In the center of Fangaia, the observed positive correlation between the conductance and temperature is not observed: here a conductive structure which obviously represents an aquifer and reaches the surface, has a temperature of <50 °C and a CO_2 flux <1000 g m^{-2} day^{-1}. The liquid water at the surface lowers the electrical resistivity explaining the observed deviation. In addition, deposits of clay-rich material at the topographically low center contribute probably to the low resistivity of this zone.

The shallow aquifer below the inner part of Solfatara is interrupted in two areas by resistive structures related to the fumaroles: firstly, a shallow resistive body (50 Ω m) between Fangaia and Bocca Grande, in a zone of high diffuse degassing at the surface, where passive seismic measurements have identified a source of high ambient seismic noise (Letort et al., 2012). Secondly, directly below Bocca Grande a gas-saturated body 'G' (50–100 Ω m) is imaged by both profiles (Figs. 3, 4) at a depth 30–100 m below the surface. This structure, interpreted as a 'plume 2' in Figs. 3, 4d, has a quasi symmetric form and is limited by a thin quasi-vertical ~20 Ω m channel (structure 'M' in Fig. 2d). This channel can be interpreted as a permeable conduit for the upflow of the water steam and carbon dioxide, consistent with high CO_2 flux and ground temperature. The location of this channel coincides with a fault orthogonal to profile 1 (Fig. 1b) which justifies a 2-D approximation for this structure, at least at the scale of the resistivity model.

Below the fumaroles, we observe a multi-layered structure which is similar to the conceptual model of the vapor-dominated system described by Ingebritsen and Sorey (1988). It is composed from the bottom to the top of: a deep conductive liquid zone of low resistivity, a large intermediate resistive gas-dominated reservoir, an upper conductive layer mainly fed by condensate, and finally an upper resistive vadose zone. Temperatures observed at Bocca Grande (160 °C) and Bocca Nuova (140 °C) correspond to saturated vapor conditions at a pressure of 6 and 4 bars, respectively, i.e. at depths of 50 and 30 m in hydrostatic regime. These depths roughly coincide with the depth of the resistive body below these fumaroles, which suggests that this gas-dominated structure represents the shallower source zone of the fumaroles.

4.2. Numerical model of the piezometric variations in Fangaia and permeability estimation

Located in the topographic minimum of Solfatara, the Fangaia mudpool is an area of pronounced variations of the piezometric surface, likely due to the gas steam condensation and hydrothermal alteration leading to reduction of permeability (Chiodini et al., 2001; Bruno et al., 2007). There is a clear coincidence between the area where water appears at the surface and the observed (5 Ω m) conductive iso-surface. Therefore we identify this iso-surface as the top of a liquid-saturated body. The presence of thermal water at the surface enhances the alteration of the tuff deposits, the permeability being nevertheless high enough to allow a high CO_2 flux with an average value of 3000 g m^{-2} day^{-1}. The 3-D model of electric resistivity below Fangaia (Fig. 6) gives a detailed image of this conductive body which we interpret as a hydrothermal plume characterized by an upwelling of the water table at kilometric scale (Bruno et al., 2007), as well as at decametric scale (this study). The shape of electrical conductive body below Fangaia is in first approximation axis symmetric with a depth that increases radially and whose top surface likely corresponds to the piezometric surface. However, several small more resistive vertical structures intersect this body (Fig. S4), and could correspond to ascending fingers of steam and CO_2, that provide condensing water at the surface. Another remarkable structure is a symmetrical ring of high CO_2 flux shown in Fig. 6 that may be due to the presence of impermeable clay deposits at the topographically low center of Solfatara crater.

Self-potential around Fangaia displays a negative anomaly. For most volcanic hydrothermal systems, negative self-potential anomalies are indicative of a presence of a subsurface downward flow (e.g., Revil et al., 1998; Revil et al., 1999b; Ishido, 2004; Revil et al., 2008; Aizawa et al., 2009). The negative anomaly of self-potential with a small positive local maximum in the center of Fangaia (Fig. 4d) might indicate the
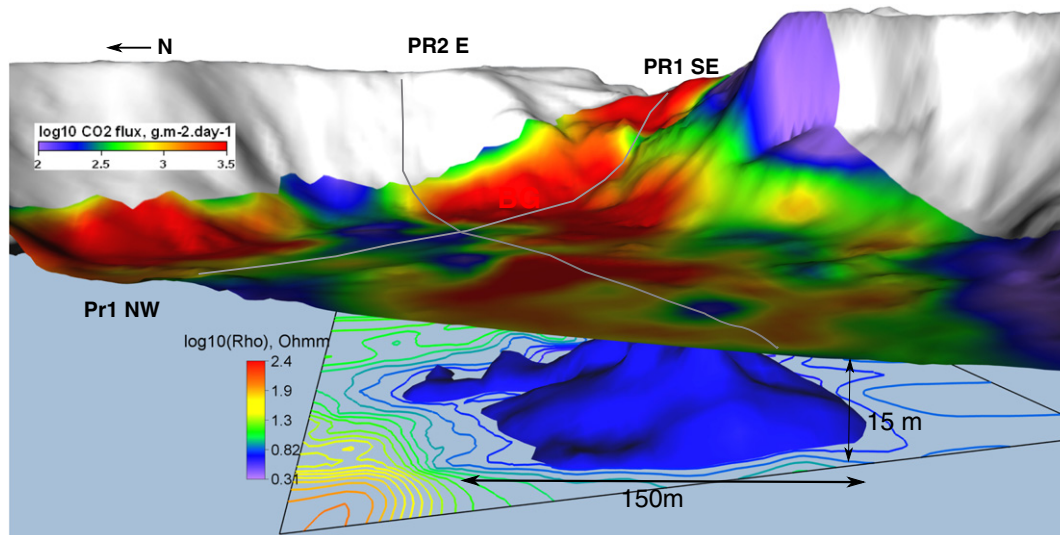

Fig. 6. Hydrothermal conductive plume below Fangaia imaged by high resolution 3-D electric resistivity tomography with a 10:1 vertical exaggeration, with a CO_2 flux color map draped on the DEM. Black rectangle indicates the extension of the 3D resistivity model, contours show electrical resistivity at 15 m depth. CO_2 scale is the same as in Figs. 2–3. The conductive plume is presented as an iso-surface of ~5 Ω m. Noteworthy are low values of CO_2 flux at the top of the plume. BG: Bocca Grande Fumarole. ERT profiles 1 and 2 are indicated in gray.
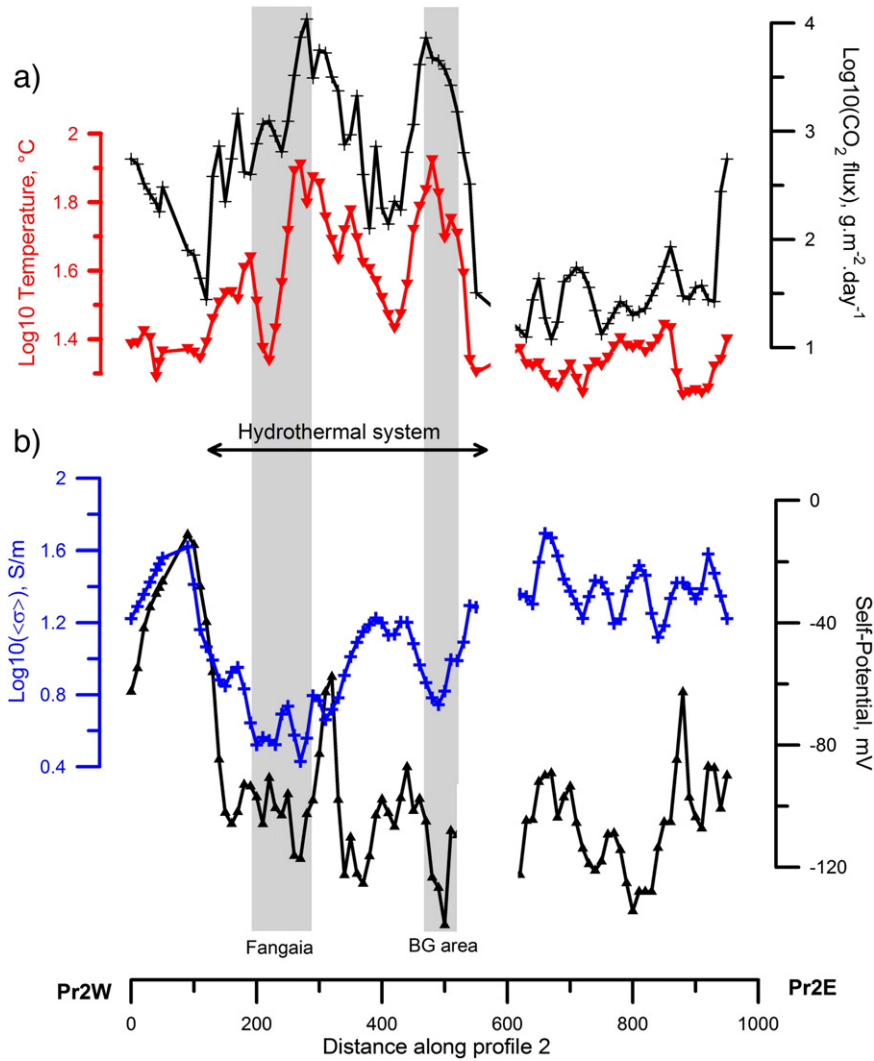
Fig. 7. Variations of a) temperature (red), CO_2 flux (black); b) conductance $<\sigma>$ (blue) and self-potential (black) along profile 2. $<\sigma>$ is the average conductivity at a depth up to 30 m, a proxy to a conductance of the shallow layer. Note the correlation between the $<\sigma>$ and gas flux and ground temperature in the hydrothermal area except for the center of Fangaia. This correlation suggests that the variations of the resistivity along this profile are rather caused by saturation and temperature variations than by lithological contrasts.
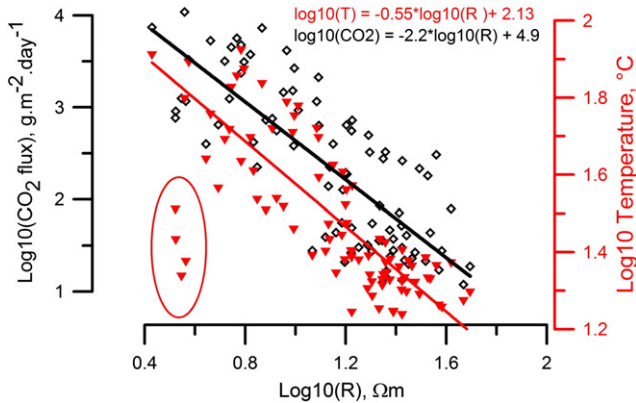

Fig. 8. Relationship between the resistance $R = 1/<\sigma>$ between 0 and 30 m, the temperature (right axis) and CO_2 flux (left axis) along profile 2 together with best fits. The points outlying from this general tendency (marked by a red ellipse) correspond to the center of Fangaia where high degree of water saturation (and consequently, low resistivity) is reached even at the surface.

coexistence of upward flow of vapor and CO_2 mixture with a descending flow of condensing liquid water. A similar observation of negative self-potential anomaly above a coupled flow of ascending CO_2/vapor and a descending liquid water was made, e.g., in a hydrothermal system in Central Nepal, where the descending flow could be evidenced by the presence of hot springs at low elevation (Byrdina et al., 2009). The electric coupling coefficient depends on water saturation and is higher for a liquid flow than for a flow of a gas–water mixture (Linde et al., 2007; Revil et al., 2007), therefore the total self-potential signal is dominated by this descending component of the flow.

4.2.1. Dupuit model I

In the following, we build a simple hydrological model inferred from resistivity, CO_2 and self-potential measurements that can explain the observed global shape of the piezometric surface below Fangaia, and we infer the mean permeability from an estimation of the condensate flow. We suppose that the flow system consists of an ascending vapor/CO_2/water mixture. CO_2 is released at the surface while the totality of the vapor condenses building a downward flow of liquid water. While the modeling of the ascending multi-phase flow is difficult, the
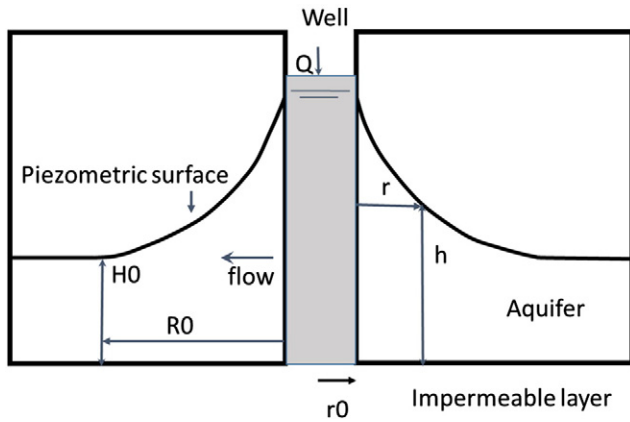
Fig. 9. Schematic drawing of an unconfined aquifer during a steady-state well pumping experiment (water injection), parameters of Dupuit equation.

modeling of the downward flow of liquid condensate is straightforward and can be reduced to the Dupuit problem of water injection in a well connected to an unconfined aquifer (Fig. 9). The Dupuit equation describes the piezometric surface created by extraction or injection of a water in an aquifer as a function of the well discharge rate and permeability (Dupuit, 1863; Bear, 1979):

$$k = \frac{Q}{\pi} \frac{\eta}{\rho_f g} \frac{\ln(r/r_0)}{(H_0^2 - h^2)}, \qquad (1)$$

where η is the fluid viscosity, ρ_f is the fluid density, g is the gravitational acceleration, and Q is the condensate injection rate (Table 1). The geometrical parameters of the Dupuit equation are shown in Fig. 9: $r_0 = 25$ m is the radius of the water saturated area at the surface, referred to as a "well"; r is the radial distance from the center of the well; h is the height of the piezometric surface at a radial distance r (Fig. 11a). The radius of action R_0 which represents the minimum radial distance from the well where the water table is not disturbed by the well action, is around 70–100 m (Figs. 6 and 3d). The water table at this radius R_0 is inferred at 15 m below the surface (Fig. 6). The depth of the aquifer $H_0 = 35$ m is the height of the water table relative to the bottom of the aquifer estimated from the resistivity contrast at the depth of 50 m (Fig. 3d).

Table 1
Physical properties used in numerical models. Parameters in the lower part of the table are identically defined for all units.

|			
Density of water	ρ_l	[kg m^{-3}]	10^3
Bulk el. conductivity (ERT data)	$\sigma(S_w = 1)$	[S m^{-1}]	0.2
Fluid conductivity (data 2013)	$\sigma_f(S_w = 1)$	[S m^{-1}]	0.75
Surface conductivity (Giberti et al., 2006)	$\sigma_f(S_w = 1)$	[S m^{-1}]	0.4
Excess of charge per unit volume	Q_{vs}	[C m^{-3}]	10^8
Dynamic viscosity	$\eta(T = 50^\circ C)$	[Pa s]	6×10^4
Dynamic viscosity	$\eta(T = 100^\circ C)$	[Pa s]	3×10^4
Porosity (Petrillio et al., 2013)	$\varnothing$		0.4
Water saturation	S_w		0.2–1
Saturation exponent	n_1		2
Apparent surface mobility of the Counterions (Revil and Florsch, 2010)	$\beta_{(s)}$	[m^2 s^{-1} V^{-1}]	$\approx 5.2 \times 10^{-9}$
Residual saturation	S_w^r		0
Van Genuchten parameter	α		0.1
Van Genuchten parameter	n		5
Van Genuchten parameter	m		$m = 1 - 1/n$
Pore connectivity parameter	L		0.5
Radius of water injection area ('Well', Figs. 9, 11a)	r_0		25
Condensate injection rate	Q	[m^3 s^{-1}]	1.6×10^{-3}
Depth of the aquifer (Figs. 9, 11a)	H_0	[m]	35
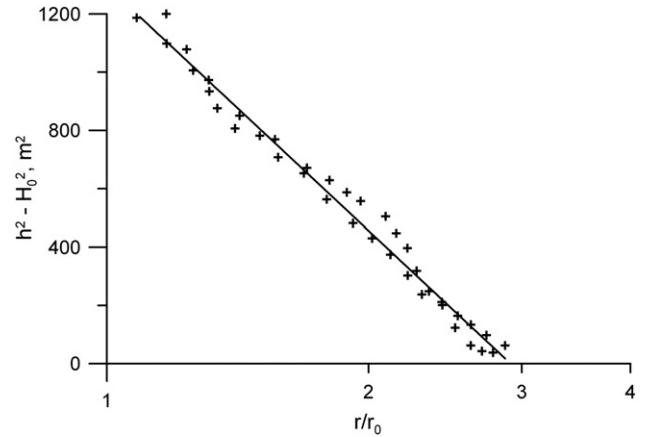
Fig. 10. Estimation of permeability using Dupuit equation (Eq. (1)) for ground water flow. Crosses show piezometric profile readings from 3-D resistivity model (Fig. 11a). The slope of the best fit (solid line), $Y = (h^2 - H_0^2/\ln(r/r_0))$, is used to solve Eq. (1).

The condensate injection rate can be calculated using the known ratio of the ascending gas mixture at Fangaia, $H_2O/CO_2 = 1.4$ (data March 2008) and an average value of the measured CO_2 flux, 3000 g m^{-2} day^{-1}. The injection rate Q of condensate across the circular area S within the radius R_0 is thus 2.3×10^2 m^3/day or $Q = 1.6 \times 10^{-3}$ m^3 s^{-1}.

We define the piezometric profile using the 5 Ω m iso-surface of the 3-D resistivity model and obtain thus the points used for graphical determination of the ratio $Y = (h^2 - H_0^2)/\ln(r/r_0)$ in Eq. (1) (Fig. 10). Eq. (1) gives the permeability of the shallow subsurface below Fangaia as 3×10^{-14} m^2 or 0.3 D.

4.2.2. Model II based on Richards equation

The Dupuit equation is based on quite strong assumptions: the vertical component of the water flow in the aquifer is neglected, and the aquifer itself is not re-alimented by the annual precipitation. In order to take into account both the vertical flow and annual precipitation, we estimate the permeability using an alternative approach. We propose a 2-D axis-symmetric numerical model of a steady-state equation of Richards for non-saturated fluid flow (Richards, 1931) using COMSOL finite element multi-physics modeling. In the central part of Fangaia the water table is set to the surface. We consider the 5 Ω m iso-surface of the 3-D resistivity model as an estimate of the piezometric surface. The resistivity is supposed to be a function of saturation only; we neglect the lithological contrasts as well as variations of temperature. We are looking for a medium permeability able to reproduce the observed profile of the piezometric surface for an input water flux Q from condensate and annual precipitation. At a given temperature, the electrical conductivity σ as function of saturation and surface conductivity σ_s can be written as (Waxman and Smits (1968); Revil and Florsch, 2010):

$$\sigma = \phi^2 S_w^2 \left(\sigma_f + \sigma_s \right) = \phi^2 S_w^2 \left(\sigma_f + \frac{\beta_{(s)} Q_{vs}}{S_w} \right) \qquad (2)$$

where ϕ is the porosity, σ_f is the fluid conductivity, Q_{vs} is the excess of surface charge per pore volume, $\beta_{(s)}$ is the apparent mobility of the counterions in the bulk pore water (Table 1). At pH exceeding the iso-electric point (pH $\approx$ 3 for silicate), the counterions are mostly cations (Revil et al., 1999a). At Solfatara, the pH is close to 6 except in the Fangaia mud-pool which is acid due to oxidation of H_2S at the surface (pH = 1.5, data 2013).

The surface conductivity (the second term in Eq. (2)) of the Neapolitan Yellow tuff samples was determined in laboratory studies as $\sigma_s \sim 0.4$ S m^{-1} (Giberti et al., 2006). Eq. (2) fits the observed surface conductivity as well as the ERT data range if we assume $Q_{vs} = 10^8$ C/m^3. As follows from Eq. (2), the surface conductivity cannot be neglected in comparison with the fluid conductivity.
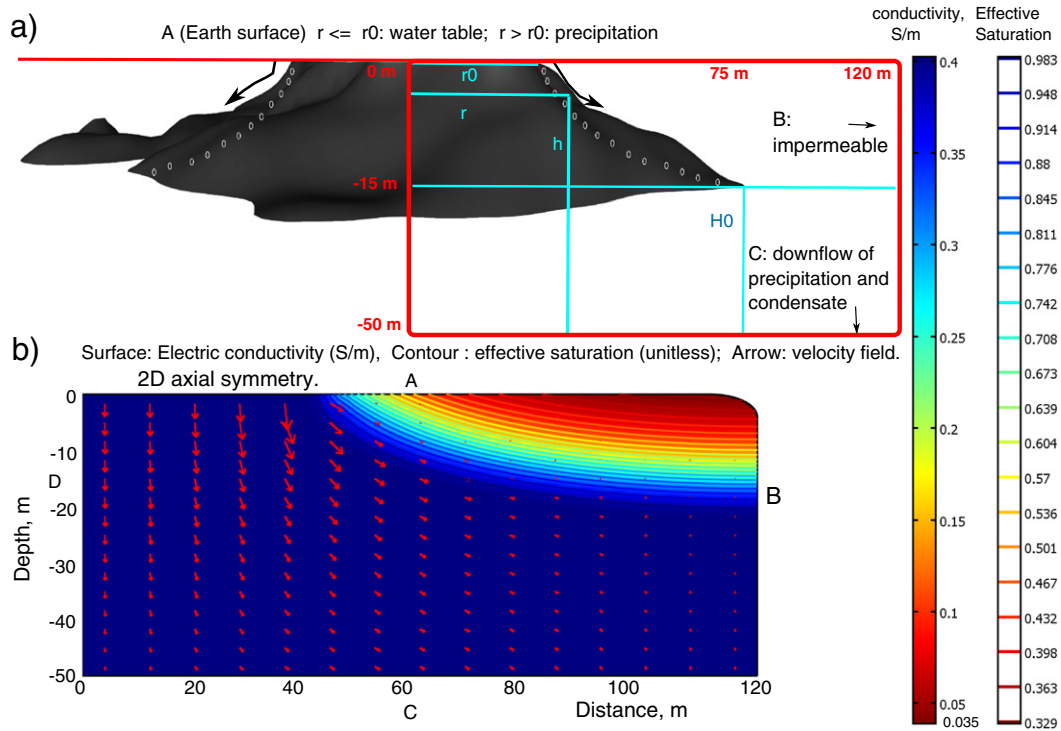
Fig. 11. Resistivity and gas saturation model of the plume displayed in Fig. 6. The orientation of the cross-section is shown by a blue line in Fig. 1. Parameters used in Dupuit equation and Fig. 10 are shown with light blue color. Red rectangle in a) highlights the limits of axis-symmetric numerical model shown in b). a) The 5 Ω m resistivity iso-surface of the 3-D model gives the position of the piezometric surface outcropping in the center area of Fangaia (the 'well' with radius $r_0 = 25$ m). On the surface, CO_2 is released to the atmosphere whereas the totality of condensing water is injected into the well. b) 2-D axis-symmetrical model of effective water saturation (contour, unitless) and conductivity (color, S/m). Boundary conditions: at the top boundary A, for $r \leq r_0$, zero pressure head; At $r > r_0$ the water flux across the boundary is given by precipitation; lateral boundary B is impermeable; at the bottom boundary C, the outward flux is given by the condensate injection rate; D: axis of symmetry.

The boundary conditions of Richards equation are: the water table level is at the surface in the center of the plume; the effective annual precipitation is given at the totality of the surface; the water table level is at 15 m depth on the sides of the plume, according to the resistivity distribution; no flow at the sides; the effective precipitation and condensate outflow are given at the bottom (Fig. 11). While the annual precipitation totals to about 1 m/year, the effective rain water infiltration is only 200 mm/year due to evaporation (see Petrillo et al., 2013, and references therein). The discretization grid of the model is shown in Fig. S7. Permeability depends on temperature via viscosity term in Eq. (S2). The resistivity of an electrolyte decreases with increase of temperature (~2% per °C, Matthess, 1982). The distribution of the temperature in the first 15 m of depth is not known and the assumption on its homogeneity is probably the strongest approximation of models I and II. Performing vertical profiles of the ground temperature (2–40 cm of depth), Chiodini et al. (2005) observed that the ground temperatures at Solfatara tend asymptotically from surface temperature to the boiling point of water. We calculate the distribution of electrical resistivity as function of saturation at two temperatures: firstly, a constant temperature $T = 50$ °C which corresponds to the average surface temperature observed at Fangaia (maximum viscosity estimation); secondly, at a constant temperature $T = 100$ °C (minimum viscosity estimation). The permeability value is estimated by trial and error fitting of the piezometric radial variations. Our numerical model allows estimating the permeability of the shallow sediments below Fangaia as 4×10^{-14} m^2 or 0.4 D for pore-water temperature of $T = 50°$, and 2×10^{-14} m^2 or 0.2 D for pore-water temperature of $T = 100°$. These results are close to the result obtained by Dupuit equation despite different simplifications. The inferred permeability belongs to the range of permeabilities $5 \times 10^{-15} - 4 \times 10^{-14}$ m^2 given by earlier laboratory studies for surface tuff samples (Giberti et al., 2006).

Model II gives a good agreement with the observed range of shallow resistivity data ($1 - 50$ Ω m, Fig. 4) despite of simplifications concerning e.g. constant temperature, geometry of the condensate flow, and perfect symmetry of the profile.

5. Conclusion

We present the results of two electrical resistivity tomography (ERT) profiles across the main features of Solfatara at Phlegrean Fields, a mapping of ground temperature, self-potential and diffuse CO_2 degassing in Solfatara area, and a detailed 3-D ERT survey of the hydrothermal plume below the Fangaia mud pool. These high resolution surveys image the hydrothermal circulation at a shallow depth and allow the quantitative modeling of the water flow below Fangaia. Globally, Solfatara can be seen as an electrical conductive area (1–200 Ω m), with flanks characterized by higher resistivity, up to 500 Ω m. We consider that the absence of resistive structures can be explained by the shallow geological structure, mainly composed of tuffs filled with hydrothermal fluids. In the inner part of Solfatara, the resistivity models suggest a two-phase hydrothermal structure below the superficial vadose zone. This hydrothermal structure consists of electrically resistive bodies at a depth of 30–100 m below the surface, which likely represent gas-dominated reservoirs feeding the fumaroles. These gas-dominated reservoirs are generally overlain by shallow conductive bodies (i.e., aquifers, filled by condensate). The deepest (down to investigation depth of 150 m below the surface) gas reservoir is found below Bocca Grande fumarole. The broad negative anomaly of self-potential found in the inner part of Solfatara, with a minimum in the area of Bocca Grande suggests a significant downward flow of condensing liquid water. The subsurface below Fangaia mud pool, located in a topographic minimum of Solfatara crater some 200 m from Bocca Grande hosts a spectacular conductive plume with typical high water saturation resistivity (< 5 Ω m). The 3-D model of the plume gives in a first approximation an axis-symmetric image of the piezometric surface. We propose a simple physical model of hydrothermal circulation below Fangaia based on Richards equation

and on an assumption that the resistivity depends on gas saturation only. Our model reproduces well the observed piezometric profile, the resistivity distribution, and allows for the estimation of the permeability of the first 15 m of depth in the range $(2 - 4) \times 10^{-14}$ m^2. This hydrothermal plume below Fangaia is surrounded by active fumaroles and represents a natural reservoir for condensing vapor. The situation can be compared with the crater of Vulcano with its cold impermeable and electrically conductive inner crater and fumaroles located at the inner part of the crater flanks (Chiodini et al., 2001; Granieri et al., 2006). In both cases, Solfatara and Vulcano, the fumaroles are located at permeable and fractured inner flanks of the crater, and the less permeable central area has a water table shallower than in the surroundings as follows from resistivity models. Water in both craters originates from precipitation and condensate. At Vulcano island, a part of the water condensing below the crater is contributing to the alimentation of the fumaroles (Chiodini et al., 2001). We can suppose a similar situation at Solfatara.

Acknowledgments

Appendix A. Supplementary data

Supplementary data to this article can be found online at http://dx.doi.org/10.1016/j.jvolgeores.2014.07.010.

References

Aizawa, K., Ogawa, Y., Ishido, T., 2009. Groundwater flow and hydrothermal systems within volcanic edifices: delineation by electric self-potential and magnetotellurics. J. Geophys. Res. 114, B01208.

Bear, 1979. Hydraulics of Groundwater. Mc Graw-Hill Inc., New York.

Bruno, P.P.G., Ricciardi, G.P., Petrillo, Z., Fiore, V.D., Troiano, A., Chiodini, G., 2007. Geophysical and hydrogeological experiments from a shallow hydrothermal system at Solfatara Volcano, Campi Flegrei, Italy: response to caldera unrest. J. Geophys. Res. 112 (B06201).

Byrdina, S., Revil, A., Pant, S.R., Koirala, B.P., Shrestha, P.L., Tiwari, D.R., Gautam, U.P., Shrestha, K., Sapkota, S.N., Contraires, S., Perrier, F., 2009. Dipolar self-potential anomaly associated with carbon dioxide and radon flux at Syabru–Bensi hot springs in central Nepal. J. Geophys. Res. 114 (B10101).

Byrdina, S., Ramos, D., Vandemeulebrouck, J., Masias, P., Revil, A., Finizola, A., Zuniga, K.G., Cruz, V., Antayhua, Y., 2013. Influence of the regional topography on the remote emplacement of hydrothermal systems with examples of Ticsani and Ubinas volcanoes, Southern Peru. Earth Planet. Sci. Lett. 365, 152–164.

Caliro, S., Chiodini, G., Moretti, R., Avino, R., Granieri, D., Russo, M., Fiebig, J., 2007. The origin of the fumaroles of La Solfatara (Campi Flegrei, South Italy). Geochim. Cosmochim. Acta 71, 3040–3055.

Chiodini, G., Frondini, F., Raco, B., 1996. Diffuse emission of CO$_2$ from the Fossa crater, Vulcano Island (Italy). Bull. Volcanol. 58, 4150.

Chiodini, G., Cioni, R., Guidi, M., Raco, B., Marini, L., 1998. Soil CO$_2$ flux measurements in volcanic and geothermal areas. Appl. Geochem. 13 (5), 543–552.

Chiodini, G., Frondini, F., Cardellini, C., Granieri, D., Marini, L., Ventura, G., 2001. CO$_2$ degassing and energy release at Solfatara volcano, Campi Flegrei, Italy. J. Geophys. Res. 106, 16,213–16,221.

Chiodini, G., Caliro, S., Cardellini, C., Granieri, D., Avino, R., Baldini, A., Donnini, M., Minopoli, C., 2005. Carbon dioxide diffuse degassing and estimation of heat release from volcanic and hydrothermal systems. J. Geophys. Res. 110 (B08204).

Chiodini, G., Caliro, S., Cardellini, C., Granieri, D., Avino, R., Baldini, A., Donnini, M., Minopoli, C., 2009. Long-term variations of the Campi Flegrei, Italy, volcanic system as revealed by the monitoring of hydrothermal activity. J. Geophys. Res. 115 (B03205).

de Siena, L., del Pezzo, E., Bianco, F., 2010. Seismic attenuation imaging of Campi Flegrei: evidence of gas reservoirs, hydrothermal basins, and feeding systems. J. Geophys. Res. 115 (B09312).

Dupuit, J., 1863. Etudes Théoriques et Pratiques sur le mouvement des Eaux dans les canaux découverts et à travers les terrains perméables. Dunod, Paris.

Finizola, A., Ricci, T., Deiana, R., Cabusson, S.B., Rossi, M., Praticelli, N., Giocoli, A., Romano, G., Delcher, E., Suski, S., Revil, A., Menny, P., Gangi, F.D., Letort, J., Peltier, A., Villasante, V., Douillet, G., Avard, G., 2010. Adventive hydrothermal circulation on Stromboli volcano (Aeolian Islands, Italy) revealed by geophysical and geochemical approaches: implications for general fluid flow models on volcanoes. J. Volcanol. Geotherm. Res. 196, 111–119.

Giberti, G., Yven, B., Zamora, M., Vanorio, T., 2006. Database on laboratory measured data on physical properties of rocks of Campi Flegrei volcanic area (Italy). In: Zollo, A., Capuano, P., Corciulo, M. (Eds.), Geophysical Exploration of the Campi Flegrei (Southern Italy) Calderas Interiors: Data, Methods and Results. Napoli, Doppiavoce, pp. 182–192 (ISBN: 978-88-89972-04-5).

Granieri, D., Carapezza, M.L., Chiodini, G., Avino, R., Caliro, S., Ranaldi, M., Ricci, T., Tarchini, L., 2006. Correlated increase in CO$_2$ fumarolic content and diffuse emission from La Fossa crater (Vulcano, Italy): evidence of volcanic unrest or increasing gas release from a stationary deep magma body? Geophys. Res. Lett. 33 (L13316).

Granieri, D., Avino, R., Chiodini, G., 2010. Carbon dioxide diffuse emission from the soil: ten years of observations at Vesuvio and Campi Flegrei (Pozzuoli), and linkages with volcanic activity. Bull. Volcanol. 72, 103–118.

Ingebritsen, S.E., Sorey, M.L., 1988. Vapor-dominated zones with hydrothermal systems: evolution and natural state. J. Geophys. Res. 93 (B11), 13 635–13 655.

Ishido, T., 2004. Electrokinetic mechanism for the, W″-shaped self-potential profile on volcanoes. Geophys. Res. Lett. 31 (L15616).

Legaz, A., Vandemeulebrouck, J., Revil, A., Kemna, A., Hurst, A., Reeves, R., Papasin, R., 2009. A case study of resistivity and self-potential signatures of hydrothermal instabilities, Inferno Crater Lake, Waimangu, New Zealand. Geophys. Res. Lett. 36 (L12306).

Letort, J., Roux, P., Vandemeulebrouck, J., Coutant, O., Cros, E., Wathelet, M., Cardellini, C., Avino, R., 2012. High-resolution shallow seismic tomography of a hydrothermal area: application to the Solfatara, Pozzuoli. Geophys. J. Int. 189, 1725–1733.

Linde, N., Jougnot, D., Revil, A., Matthäi, S., Arora, T., Renard, D., Doussan, C., 2007. Streaming current generation in two-phase flow conditions. Geophys. Res. Lett. 34 (L03306).

Lirer, L., Petrosino, P., Alberico, I., Armiero, V., 2011. Carta geologica del vulcano Solfatara. I Campi Flegrei: storia di un campo vulcanico. 57. Quaderni dell'Accademia Pontaniana, Naples, p. 178 (ISBN: 9788874315147).

Loke, M., Barker, R.D., 1996. Rapid least-squares inversion of apparent resistivity pseudosections by a quasi-Newton method. Geophys. Prospect. 44, 131–152.

Matthess, 1982. The Properties of Groundwater. John Wiley & Sons, New York.

Petiau, 2000. Second generation of lead–lead chloride electrodes for geophysical applications. Pure Appl. Geophys. 157, 357–382.

Petrillo, Z., Chiodini, G., Mangiacapra, A., Caliro, S., Capuano, P., Russo, G., Cardellini, C., Avino, R., 2013. Defining a 3D physical model for the hydrothermal circulation at Campi Flegrei caldera (Italy). J. Volcanol. Geotherm. Res. 264, 172–182.

Revil, A., Florsch, N., 2010. Determination of permeability from spectral induced polarization in granular media. Geophys. J. Int. 181, 1480–1498.

Revil, A., Cathles, L.M., Losh, S., Nunn, J., 1998. Electrical conductivity in shaly sands with geophysical application. J. Geophys. Res. B10, 23925–23936.

Revil, A., Pezard, P.A., Gloverx, P.W.J., 1999a. Streaming potential in porous media 1. Theory of the zeta potential. J. Geophys. Res 104, 20021–20031.

Revil, A., Schwaeger, H., Cathles, L.M., Manhardt, P.D., 1999b. Streaming potential in porous media 2. Theory and application to geothermal systems. J. Geophys. Res. 104, 20033–20048.

Revil, A., Finizola, A., Sortino, F., Ripepe, M., 2004. Geophysical investigations at Stromboli volcano, Italy. Implications for ground water flow and paroxysmal activity. Geophys. J. Int. 157 (1), 426–440.

Revil, A., Linde, N., Cerepi, A., Jougnot, D., Matthäi, S., Finsterle, S., 2007. Electrokinetic coupling in unsaturated porous media. J. Colloid Interface Sci. 313, 315–327.

Revil, A., Finizola, A., Piscitelli, A., Rizzo, E., Ricci, T., Crespy, A., Angeletti, B., Balasco, M., Barde-Cabusson, S., Bennati, L., Bolve, A., Byrdina, S., Carzaniga, N., Gangi, F.D., Morin, J., Perrone, A., Rossi, M., Roulleau, E., Suski, B., 2008. Inner structure of La Fossa di Vulcano (Vulcano Island, southern Tyrrhenian Sea, Italy) revealed by high resolution electric resistivity tomography coupled with self-potential, temperature, and soil CO$_2$ diffuse degassing measurements. J. Geophys. Res. 113 (B07207).

Revil, A., Finizola, A., Ricci, T., Delcher, E., Peltier, A., Barde-Cabusson, S., Avard, G., Bailly, T., Bennati, L., Byrdina, S., Colonge, J., Gangi, F.D., Douillet, G., Lupi, M., Letort, J., Sun, E.T. H., 2011. Hydrogeology of Stromboli volcano, Aeolian Islands (Italy) from the interpretation of resistivity tomograms, self-potential, soil temperature and soil CO$_2$ concentration measurements. Geophys. J. Int. 186, 1078–1094.

Richards, L., 1931. Capillary conduction of liquids through porous media. Physics 1, 318–333.

Rinaldi, A., Todesco, M., Vandemeulebrouck, J., Revil, A., Bonafede, M., 2011. Electrical conductivity, ground displacement, gravity changes, and gas flow at Solfatara crater (Campi Flegrei caldera, Italy): results from numerical modeling. J. Volcanol. Geotherm. Res. 207, 93105.

Todesco, M., Rinaldi, A.P., Bonafede, M., 2010. Modeling of unrest signals in heterogeneous hydrothermal systems. J. Geophys. Res. 115, B09213.

Valentino, G., Cortecci, G., Franco, E., Stanzione, D., 1999. Chemical and isotopic compositions of minerals and waters from the Campi Flegrei volcanic system, Naples, Italy. J. Volcanol. Geotherm. Res. 91, 329–344.

Waxman, M.H., Smits, L.J.M., 1968. Electrical conductivities in oil-bearing shaly sand. Soc. Petrol. Eng. J. 8, 107–122.

Zohdy, A.A.R., Anderson, L., Muffler, L., 1973. Resistivity, self-potential, and induced-polarization surveys of a vapor-dominated geothermal system. Geophysics 38, 1130–1144.

Zollo, A., Maercklin, N., Vassallo, M., Iacono, D.D., Virieux, J., Gasparini, P., 2008. Seismic reflections reveal a massive melt layer feeding Campi Flegrei caldera. Geophys. Res. Lett. 35, L12306.